Journal of Molecular Catalysis A: Chemical 301 (2009) 98–105

Contents lists available at ScienceDirect

Journal of Molecular Catalysis A: Chemical

journal homepage: www.elsevier.com/locate/molcata

Catalyst deactivation during hydrogenation of carbon dioxide: Effect of catalyst position in the packed bed reactor

Sung-Chul Lee[a,*], Jun-Sik Kim[a], Woo Cheol Shin[a], Myung-Jae Choi[b], Suk-Jin Choung[c]

[a] Samsung SDI Co. Ltd., 575 Shin-dong, Yeongtong-gu, Suwon-si, Gyeonggi-do 443-391, Republic of Korea
[b] Chemical Technology Division, Korea Research Institute of Chemical Technology, Daejon 505-600, Republic of Korea
[c] College of Environment and Applied Chemistry, Kyung Hee University, Gyeonggi 449-701, Republic of Korea

ARTICLE INFO

Article history:
Received 12 August 2008
Received in revised form
12 November 2008
Accepted 13 November 2008
Available online 24 November 2008

Keywords:
CO_2 hydrogenation
Fe–K/γ-Al_2O_3
Deactivation
Iron phase

ABSTRACT

To examine the deactivation pathway of Fe–K/γ-Al_2O_3 catalyst in CO_2 hydrogenation, XPS, HR-TEM, TPO, Mössbauer spectroscopy, and reaction studies were conducted. The iron-based catalysts were deactivated significantly during CO_2 hydrogenation because of catalyst poisoning and carbon deposit. The characterizations of deactivated catalyst were also carried out to provide information on the deactivation pathway as a function of time and catalyst position. The deactivation occurred on Fe–K/γ-Al_2O_3 during the reaction although the long run activity was above 35%. The deactivation pathway was different according to the reactor position. As time progressed, hematite (Fe_3O_4), formed after H_2 reductions, was gradually carburized to χ-Fe_5C_3. Finally, χ-Fe_5C_3 phase was converted to θ-Fe_3C, which is inactive species for CO_2 hydrogenation. The main deactivation reason at the inlet part in the reactor was phase transformation. Conversely, the main factor at the outlet part in the reactor was the coke deposit generated by secondary reactions.

1. Introduction

The Fischer–Tropsch Synthesis (FTS) has been extensively investigated since the discovery of methane production over nickel in 1902. Over the past three decades, the hydrogenation of carbon monoxide (CO) was actively studied all over the world because it is an important step in utilizing coal and natural gas as carbon sources [1,2]. On the other hand, hydrogenation of carbon dioxide (CO_2) received much less attention, partly because of the unfavorable thermodynamic considerations. In recent years, however, various kinds of chemical processes have been tried to turn CO_2 into valuable chemical compounds, attracting much attention to this chemical process as a promising solution for the future.

The catalytic activity and selectivity in CO_2 hydrogenation are dependent on the phase of iron metal. During the CO_2 hydrogenation or pretreatment, the phases of catalysts are transformed. Many reports [3–7] have investigated the phase transformation of iron-based catalyst in FTS. Characterization technologies of in-situ Raman spectroscopy, in-situ magnetic measurements, or Mössbauer spectroscopy were used to characterize the phase transformation of iron catalysts.

Compared to FTS studies, there is very little literature investigating the role of different iron phases in CO_2 hydrogenation. To understand how iron catalysts can be applied to CO_2 hydrogenation effectively, the role of different iron phases was investigated through FTS in this study.

There are a number of studies on iron catalysts concerning the role of iron phases in CO hydrogenation. The two models, which are most frequently cited, are the carbide model and competition model. Dictor and Bell [3] suggested that ε′-$Fe_{2.2}C$ is the active phase on iron-based catalysts. Based on Mössbauer spectroscopy, Niemantsverdriet et al. [4] and Butt and coworkers [5] proposed that iron carbide is the active sites. Shroff et al. [6] have concluded that the transformation of magnetite into iron carbides is needed for a FT activity. Another model [7] proposed that two active sites operate simultaneously on the surface of iron catalysts: Fe0/Fe-carbides and iron oxide (Fe_3O_4). The carbide phase is active toward dissociation of CO and formation of hydrocarbons, whereas the oxide phase adsorbs CO associatively and produces oxygenated products. The ε-carbide or χ-carbide is the active form of iron catalysts. A principal cause of iron catalyst deactivation is the transformation of active surface carbon species and/or active iron carbide phases to inactive carbon or carbide forms that foul or poison the surface. As time progresses, in the case of CO hydrogenation, the χ-carbide is gradually oxidized to magnetite. As a result of this transformation in the catalyst surface compositions, the catalyst activity is deactivated.

Three types of catalyst deactivation behaviors were investigated in this paper. First, the durability of the catalysts was studied by measuring the activation behavior after 500 h under identical conditions. The differences in carbon dioxide conversion, product

* Corresponding author. Tel.: +82 31 210 7074; fax: +82 31 210 7374.
E-mail address: sungchul01.lee@samsung.com (S.-C. Lee).

1381-1169/$ – see front matter © 2008 Elsevier B.V. All rights reserved.
doi:10.1016/j.molcata.2008.11.016

selectivity, reactor temperature and other factors were measured to observe the change in activation behavior. Second, changes in the catalyst surface and change in activation behavior at the various catalyst layers in the reactors were tracked over time to study the decrease in catalyst activation more accurately. Through the surface characteristics of the active species, the phase transformation that occurs during the deactivation process of the active species was estimated. Lastly, the carbon deposition that arose due to the carburization of the hydrocarbon at the active sites was studied. Qualitative and quantitative analyses for the amount of carbonaceous species were needed for catalyst regeneration.

2. Experimental

2.1. Catalyst preparation

Fe–K/γ-Al_2O_3 catalysts were prepared by the impregnation of γ-Al_2O_3 with aqueous solutions of $Fe(NO_3)_3{\cdot}9H_2O$ and K_2CO_3 [8]. The nominal catalyst compositions were 1.00Fe/0.35K/5.00Al_2O_3. The impregnated catalysts were homogeneously mixed, and a small amount of water was added. Pellets, 3 mm in length, were extruded through a 1.5-mm-diameter die. These pellets were dried at 393 K for 12 h and calcined at 773 K for 24 h in air.

2.2. Characterization

X-ray powder diffraction was used to examine the crystallinity of the catalysts. Diffraction patterns were collected at 10°/min intervals on a Rigaku 2155D6 X-ray diffractometer with a CuKα X-ray source. The BET surface area was measured using Micrometrics ASAP 2000. All catalysts were degassed before the measurement. The degassing was carried out under vacuum at 393 K for 3 h and then 573 K for 5 h. To analyse the binding energy, X-ray photoelectron spectroscopy (XPS, PHI 5700, PHI com.) was employed. Fresh catalysts were prepared with pellets of 5 mm in length and treated in vacuum overnight prior to the measurement. The Al mono (pass energy = 23.5 eV) was used as an X-ray source at 350 W power, 15 kV, and pressure was kept below 2.7×10^{-6} Pa during the measurement.

Mössbauer spectra were recorded, using a constant acceleration spectrometer of ^{57}Co radioactive source in a Rh matrix. Mössbauer spectra were analyzed, using a program based on the distribution of hyperfine magnetic field and quadruple splitting. Scanning electron microscopy (SEM) was done to investigate the coke morphology of samples.

The coked samples were submitted to a soxhlet extraction treatment with dichloromethane for 24 h. Thermogravimetric analyses were performed in a TA instrument on 10–15 mg of sample under a flow of He (50 sccm) at 10 K/min to 573 K for 1 h to remove adsorbed moisture and other species. After pretreatment, the sample under a flow of air (50 sccm) was heating at 10 K/min from room temperature to 973 K.

2.3. Catalyst activity

CO_2 hydrogenation was carried out in a bench scale fixed bed reactor (1.6 cm-ID × 60 cm-high). A schematic diagram of the fixed bed reactor system used is shown in Fig. 1. The reaction and internal standard gases (CO_2, H_2, N_2, He) were taken from cylinders and their flow rates were controlled by using a mass flow controller (MFC). Reaction temperature was controlled at 573 K and reaction pressure was maintained at 10 atm by using a back pressure regulator (BPR).

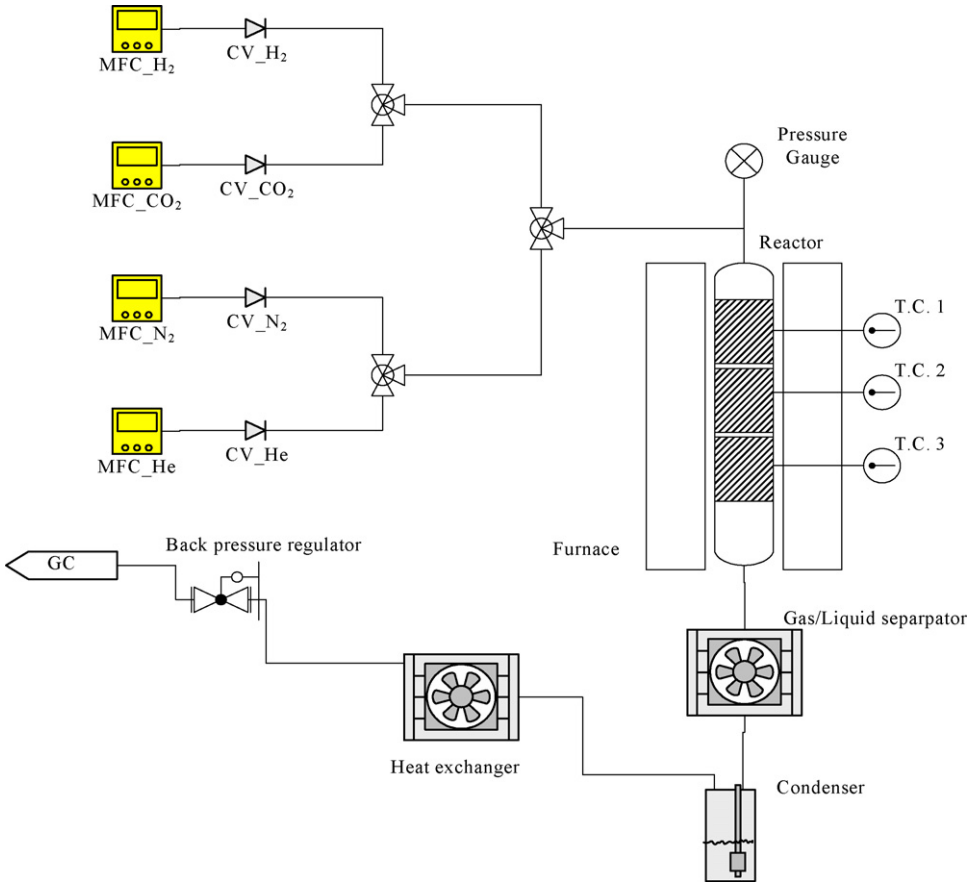

Fig. 1. Experimental apparatus.

21.0 g of catalysts were filled up and the flow rate of the mixed gas was 2000 ml/g_{cat} h at STP. The gas composition ratio was three parts H_2 to one part CO_2. The liquid products were separated from gas products in the gas–liquid separator and condenser. The exit gas flow rate was measured by a digital bubble flow meter to evaluate the reaction conversion. The gaseous products were analyzed using two types of on-line GC-TCD, which used standard gases, N_2 and He, internally to check the consumption of CO_2 and H_2. With the data obtained from the GC-TCD analysis, the conversion of CO_2 and the yield of CO and CH_4 were calculated. The peak areas of organic products were inferred from the peak areas of CH_4 (GC-TCD); the organic product selectivity and yields were determined from the GC-FID analysis.

3. Results and discussion

3.1. Deactivated behavior in hydrogenation of carbon dioxide

The Fe–K/γ-Al_2O_3 catalyst promoted hydrogenation of carbon dioxide and generated partially reduced carbon monoxide or methane, and fully hydrogenated hydrocarbons. The reaction rate of CO_2 hydrogenation over a Fe–K/γ-Al_2O_3 catalyst, obtained by reducing 21 g of the fresh catalyst, was determined as a function of time at 573 K and is given in Fig. 2. Rates are expressed as the number of moles of CO_2 reacted to the CO, H_2O, and hydrocarbons produced per gram of catalyst per hour. The reaction rate started at zero and reached a maximum value after 50 h, then the rate fell to a level of 12% of the maximum due to deactivation after 500 h.

The reactor position and time-dependent behavior of a Fe–K/γ-Al_2O_3 catalyst during CO_2 hydrogenation at 573 K was studied using the following procedures. A sample, obtained by reducing 21 g of the fresh catalyst, was subjected to synthesis for 100 h. After the sample of distinct stage was removed from the reactor, a new sample was introduced and subjected to the reaction process for a longer time. This process was repeated. Reaction rates and product distributions were measured as a function of time for each experiment. For the analysis of the catalyst used as a function of reaction times and reactor positions, the reaction rates of identical samples were measured, then the used samples of distinct stages were obtained at 100, 300 and 500 h intervals. No significant differences among these experiments were found for the corresponding intervals. Hence, the reaction process was sufficiently reproducible to justify usage in the study of catalyst time dependence.

CO_2 hydrogenation reaction was induced using a one-dimensional reactor with a constant inlet temperature (573 K).

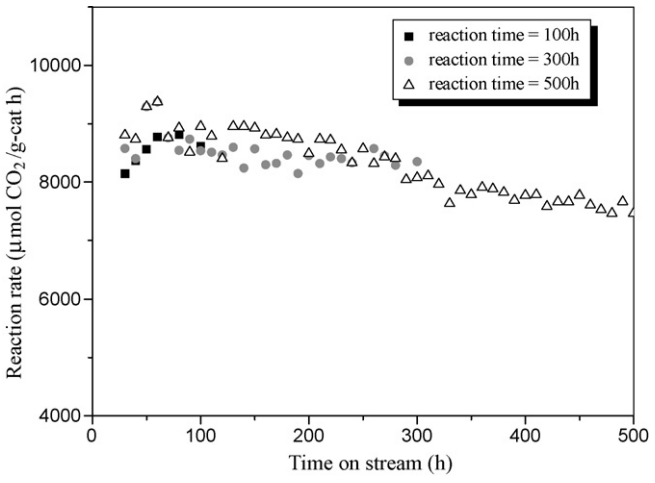

Fig. 2. Catalytic activity of CO_2 hydrogenation, reaction conditions: T = 573K, P = 10 atm, S.V. = 2000 ml/g_{cat} h, H_2/CO_2 = 3.

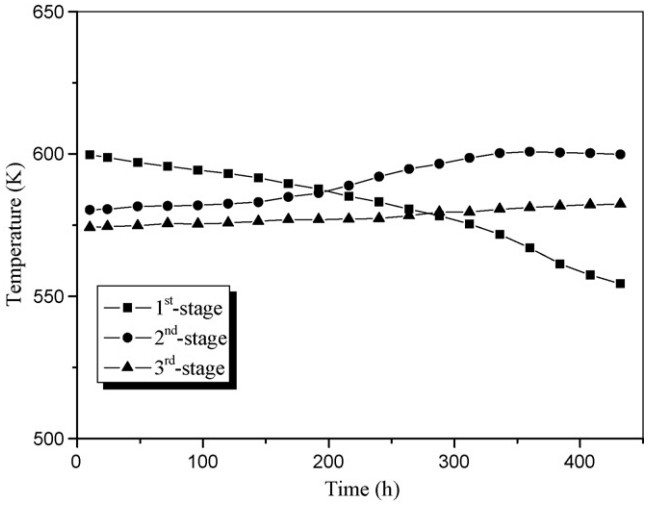

Fig. 3. Temperature profile of reactor with time on stream.

Temperature profiles were recorded at the indicated axial positions in the reactor bed. Fig. 3 shows the typical temperature profiles in the axial direction. The temperature profiles for every stage were quite different from each other. The initial reaction temperature in a 1st-stage bed reached 600 K, although the inlet temperature was 573 K. It decreased as the reaction time became longer. However, the reaction temperature in a 2nd-stage bed stayed within the range of 573–583 K for the initial 200 h, and then it started to increase rapidly. It reached a steady state after 300 h. As the reaction continued, the maximum temperature location of the reactor shifted to the lower position of the reactor. This shift of the maximum temperature location with reaction time was caused by the deactivation of catalysts. The 1st-stage catalysts in the initial reaction were deactivated over 300 h, then the active species in the 1st-stage catalysts disappeared after 300 h. Therefore, the main reaction zone shifted to the catalysts zone in the 2nd-stage reactor.

The effect of the reaction time on hydrocarbon product distribution is shown in Table 1 and Fig. 4. Hydrocarbon products in Fig. 4 are lumped into four groups: methane (C_1), light gases (C_2–C_4), gasoline fraction (C_5–C_{11}), and diesel fuel and hydrocarbon wax (C_{12+}). The Fe–K/γ-Al_2O_3 catalyst had a low methane selectivity (~10 wt%). As time progressed, the hydrocarbon selectivities of methane and C_2–C_4 hydrocarbon were similar, whereas C_5–C_{11} selectivity decreased. This result was in agreement with previous studies [9–11], indicating that the amount of iron carbide (χ-Fe_5C_2 and θ-Fe_3C) increased with reaction time, and that the parallel rise in the rate of C_{12+} hydrocarbon formation and inactive carbide content of the catalyst is due to the fact that hydrocarbons and carbides are formed from the progressive accumulation of a common precursor.

3.2. Consideration of active species

X-ray powder diffraction pattern of Fe–K/γ-Al_2O_3 catalyst with reactor position after 100, 300 and 500 h of CO_2 hydrogenation is

Table 1
The product distribution of CO_2 hydrogenation.

Reaction time (h)	CO (%)	Hydrocarbon (%)				Others (%)
		CH_4	C_2–C_4	C_5–C_{11}	C_{12+}	
100	10.7	5.9	18.1	26.8	18.2	20.2
300	12.4	6.2	16.8	26.6	19.4	18.6
500	13.3	6.5	17.1	23.8	21.4	18.0

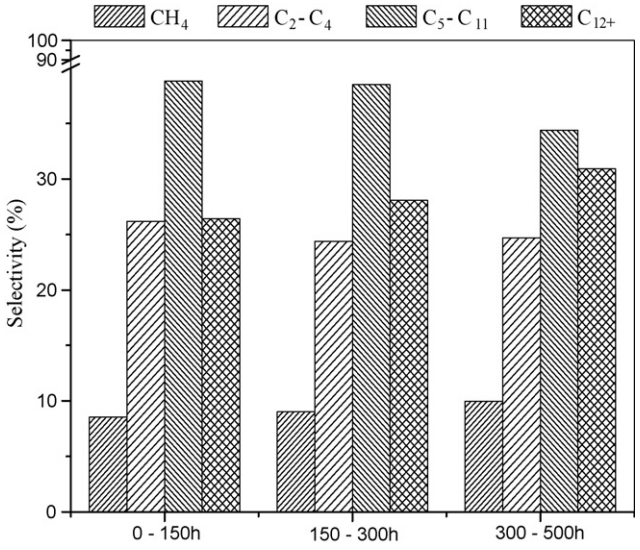

Fig. 4. Effect of reaction time on hydrocarbon distribution.

shown in Fig. 5. The iron phase of the deactivated catalyst consisted of iron carbides (χ-Fe_5C_2 and θ-Fe_3C) and magnetite (Fe_3O_4). The diffraction peaks at $2\theta = 36.8^\circ$ and 59.3° correspond to Fe_3O_4, and the diffraction peaks at $2\theta = 45.1^\circ$ and 50.7° are due to χ-Fe_5C_2, which has been known as an active phase in FTS. The patterns in Fig. 5 show that the iron carbide and magnetite peaks are seen at 2θ values of 45.1°, 50.7°, 43.7°, 37.8°, 36.8° and 59.3° [8]. In the XRD results, the γ-Al_2O_3 peak at 66.5°, which is used as supporter, remained relatively unchanged. The γ-Al_2O_3 peak was used as an internal standard to approximate the amount of the main phases. The amount of Fe_3O_4 in every stage decreased as the reaction time became longer. In the case of χ-Fe_5C_2, the amount reached a maximum value after 300 h, and then the amount decreased slightly after 500 h. Because the peaks of iron carbide and magnetite overlap, it was very difficult to exactly quantify the amounts of various phases by means of XRD analysis. To overcome this difficulty in the iron phase of deactivated catalysts, Mössbauer spectroscopy was measured. Mössbauer spectroscopy has yielded extremely useful information on a number of important catalysts, such as iron catalyst for Fischer–Tropsch and ammonia synthesis, and cobalt–molybdenum catalyst for hydrodesulfurization reactions. Fig. 6 represents the Mössbauer spectrum of Fe–K/γ-Al_2O_3 after being subjected to the reaction condition at 573 K for 300 h. The overall spectra were deconvoluted with calculated Mössbauer spectra that consisted of Lorentzian-shaped lines. In the case of quadruple doublets, the line width and the absorption areas of the constituent lines were constrained equally. The magnetically split lines were fitted with several components in order to simulate a distribution of hyperfine fields. All spectra were collected at room temperature following each stage with the sample, and the solid

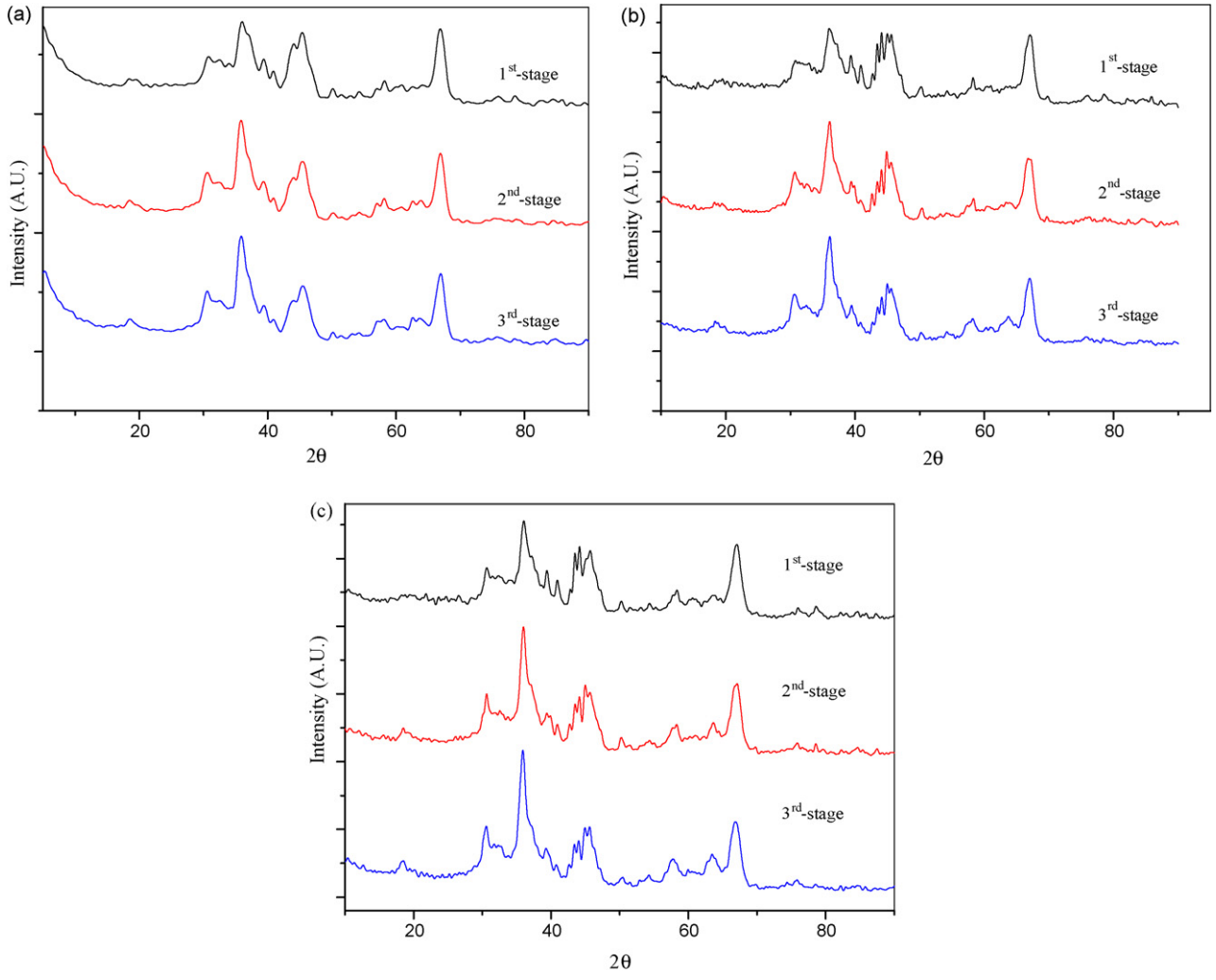

Fig. 5. XRD profiles of Fe–K/γ-Al_2O_3 catalysts with time on stream. (a) 100 h, (b) 300 h, and (c) 500 h.

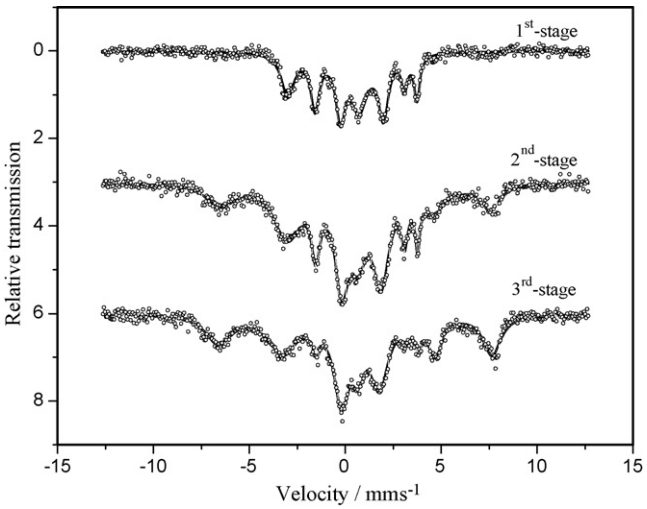

Fig. 6. Mössbauer spectra of the Fe–K/γ-Al_2O_3 with reactor position.

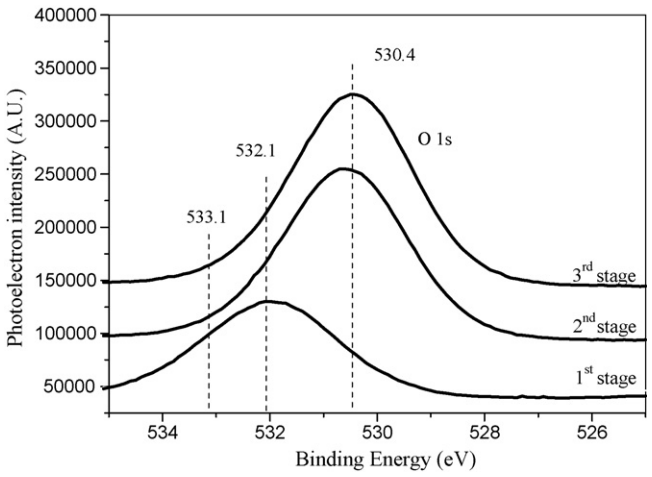

Fig. 7. Oxygen 1s XPS spectra of the Fe–K/γ-Al_2O_3 with reactor position.

lines through the data points are the optimized fits obtained with the corresponding spectral contributions. The calcined catalyst was reduced to Fe_3O_4 and also carburized to χ-Fe_5C_2 and θ-Fe_3C during CO_2 hydrogenation. The spectral contribution was calculated from the percentage area under each spectral component. θ-Fe_3C was the major solid phase detected in the used 1st-stage catalyst after 300 h (67.3%) followed by χ-Fe_5C_2 (27.1%), while Fe_3O_4 contribution was only 5.6%. However, in the case of the used 3rd-stage catalyst after 300 h, the amount of Fe_3O_4 and χ-Fe_5C_2 increased, and the amount of θ-Fe_3C, which was the inactive species, decreased to 19.4%. The Mössbauer spectra presented in Fig. 6 indicates that after 300 h of reaction, the Fe–K/γ-Al_2O_3 in 1st-stage bed contained considerably more θ-Fe_3C than that in the 2nd- and 3rd-stage bed. These observations suggest that Fe_3O_4, which is reduced, transforms into χ-Fe_5C_2, and then χ-Fe_5C_2 subsequently transformed completely to the inactive species (θ-Fe_3C). From these results, it is estimated that the deactivation of Fe–K/γ-Al_2O_3 catalyst in CO_2 hydrogenation is attributed to the phase transformation of the active species.

Fig. 7 shows the O 1s region for the used catalysts after 300 h. For the catalyst in the bottom bed, the signal peak at a binding energy of 530 eV was related to the lattice O^{2-} of metal oxide. In the case of 1st-stage catalyst, the intermediate state was observed for the formate, characterized by O 1s peaks at 532.1 and 533.1 eV [12,13]. The O 1s spectrum was deconvoluted into three peaks centered at 530.4, 532.1 and 533.1 eV. The peak at the higher binding energy was assigned to the carbonyl oxygen. According to the surface composition of the catalyst at each stage, the total oxygen concentration should also include metal oxide and carboneous species; the existence of the latter has been suggested on the basis of C 1s region. The surface composition was calculated from the XPS peak areas using atomic sensitivity factors: 3.00 for Fe ($2p_{3/2}$), 0.66 for O (1s), 0.18 for Al (2p), 1.24 for K (2p), and 0.25 for C (1s). The major species in the 1st-stage catalyst bed was carboneous species. With the lower stage, however, there was an increasing trend in the amount of oxide. In the 1st-stage catalyst bed, which has been reacted severely, the main species on the surface composition was a carboneous group (Table 2). From these results, the reaction pathway is estimated as shown in Scheme 1. At the beginning of the reaction, the active site, which was Fe_3O_4, and CO_2 underwent a series of reactions according to Scheme 1. Compared with O 1s XPS results, the main catalytic surface composition in a 1st-stage bed is C–O and C=O group due to the carboneous group. In the case of a 3rd-stage bed, metal oxide was the dominant species. It is estimated that the active species of reverse water gas shift (RWGS)

Table 2
XPS results of catalysts with catalytic bed positions.

	Fe	O			K		C				Al
		Oxide	Carbonyl	Hydroxyl	Oxide	Metal	Graphite	Iron carbide	HC	Formate	
1st-Stage	1.48	–	13.2	14.58	0.08	1.36	22.5	11.3	17.4	6.7	11.32
2nd-Stage	1.65	39.51	3.33	2.16	3.39	0.3	13.7	2.7	9.1	4.2	19.91
3rd-Stage	1.47	45.58	3.27	–	4.17	0.08	7.3	2.6	9.2	4.0	22.31

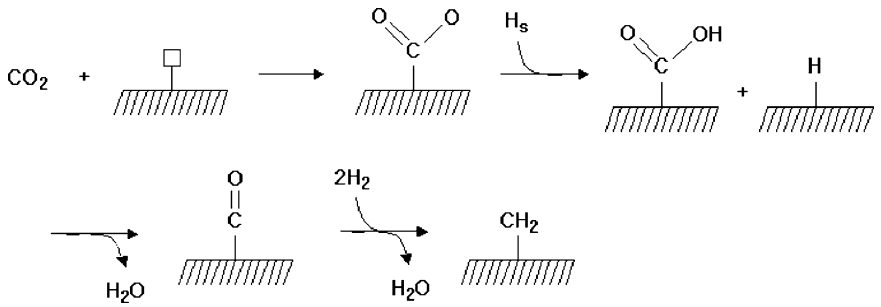

Scheme 1. Proposed mechanism of CO_2 hydrogenation over Fe–K/γ-Al_2O_3 catalyst.

reaction was magnetite, and then the magnetite was transformed into iron carbide during CO_2 hydrogenation.

According to the results of Mössbauer spectrum and XRD, the active catalytic phase in CO_2 hydrogenation may be Fe_3O_4, which converted over a long period of reaction time to χ-carbide. Then χ-Fe_5C_2 transformed to θ-Fe_3C. This is a reasonable scheme, considering that the order of increasing thermal stability for iron phases is χ-Fe_5C_2 < θ-Fe_3C; and that Fe–C bond strength increases in the same order. Therefore, it is concluded that the carboneous group was formed by reaction with CO_2, and that the carboneous group was transformed to adsorbed CH_2 during CO_2 hydrogenation. Adsorbed CH_2 was converted to χ-carbide over long periods of CO_2 hydrogenation, and finally the χ-carbide was transformed to the stable carbide, which was the deactivated species in CO_2 hydrogenation.

When iron oxide catalysts were exposed to FT synthesis reaction environments, the catalyst transformed from hematite into one or more carbides. After performing FT synthesis on the precipitate, an unsupported iron oxide catalyst, Shroff et al. [6] observed that the single crystals of hematite first transformed into magnetite retaining the characteristic Swiss cheese morphology, and that the carbide phase was then formed as small nodules on the surface of the magnetite with the phase transformation proceeding slowly into the bulk. Finally, the breakdown of the original single crystals was brought about by this phase transformation.

3.3. Characterization of the deposited species

The carbon mass balance obtained in the presence of catalyst have to be close to 100% for Fe–K/γ-Al_2O_3 catalyst, but the 20% deficit existed mainly due to carbon deposition and oxygenate compounds (Table 1). It should be mentioned that traces of oxygenate compounds were also observed on some chromatograms, among which alcohols were identified but not quantified. Therefore, thermogravimetric analysis of the samples was carried out to estimate coke deposit as revealed by the reduction in weight due to coke oxidation in air. The TG/DTG profiles of the used catalysts are given in Fig. 8. In the TGA analysis, a first weight loss is observed below 473 K, produced by water desorption. Thermograms of the used catalysts exhibit two distinct coke oxidation temperature regions corresponding to metal and support sites [14–16]. The low temperature region (523–673 K) consisted of coke species deposited on metal sites. In the high temperature region, coke on the support that contains more polymerized/condensed coke species, got oxidized at a higher temperature, between 673–773 K. Fig. 8 shows that the deposition of coke on metal sites for all deactivated catalysts, whereas the 1st-stage samples show that the coke deposition only occurred in the high temperature region. The 3rd-stage sample, which reacted for 500 h, showed a desorption peak at 773 K. In the case of TG profiles, it was observed that there were a 20% and 7% weight loss for a 1st-stage sample and a 2nd-stage sample

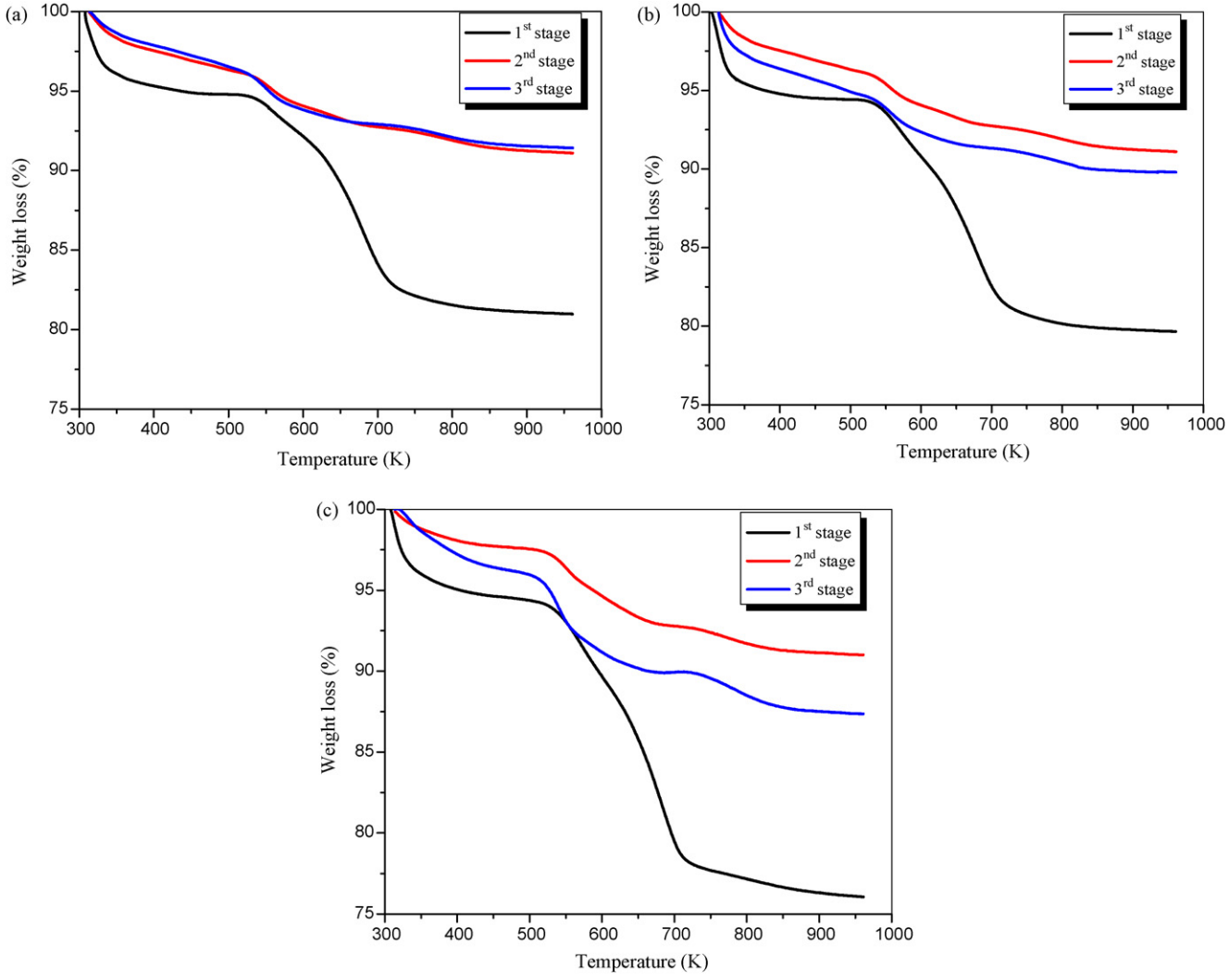

Fig. 8. TG profiles of the Fe–K/γ-Al_2O_3 catalysts after CO_2 hydrogenation reaction. (a) 100 h, (b) 300 h, and (c) 500 h.

Table 3
Surface area of Fe–K/γ-Al_2O_3 catalyst at T = 573 K after reaction for 300 h.

	BET surface area (m^2/g)	Pore volume (cm^3/g)
Fresh	82.3	0.28
1st-Stage	62.9	0.25
2nd-Stage	82.4	0.28
3rd-Stage	86.4	0.28

respectively. However, there was a 10% weight loss for a 3rd-stage sample. Comparing this with the DTA results, it is believed that the produced hydrocarbons in previous stages were deposited at the catalyst in 3rd-stage, hence the coke in the 3rd-stage was denser than the other samples.

As shown in Table 3, the surface areas of catalysts in 1st-, 2nd- and 3rd-stages were 62.9, 82.4 and 86.4 m^2/g, respectively. In the 1st-stage, it was decreased significantly compared to that of fresh catalyst. There was no significant difference in the surface area of 2nd-stage catalyst. However, the surface area of the 3rd-stage catalyst was increased slightly. With the lower stages, there was an increasing trend in the surface area of catalyst. From these results, in the 1st-stage, the filamentous coke was formed on the catalyst and required the participation of active site. However, polymeric coke formed in 2nd- and 3rd-stages was derived from gas-phase decomposition of hydrocarbon.

The SEM micrographs of the used catalysts (Fig. 9), clearly showed differences in the amount of coke deposited on the three samples, and also in the coke structure. In the 2nd- and 3rd-stage catalyst (Fig. 9b and c), the amount of coke deposited (determined by Fig. 8) was very low while a noticeable coke coverage of the 1st-stage catalyst (Fig. 9a) was observed. In the case of samples in different stages and reaction time, two kinds of graphite were identified as shown in Fig. 9. One consisted of filamentous graphite, which was found only scarcely. Most of the surface was covered by the other kind which consisted of two parts, deposited graphite and graphite clusters protruding on the surface mixed with some fine filamentous carbon [17]. The SEM back-scatter electron image showed many bright points distributed uniformly in these graphite clusters. After 150 h of reaction, the graphite clusters grew further to form bigger graphite clusters (Fig. 9). In this case, no filamentous carbon was found. Furthermore, increasing the reaction time to 500 h did not change the graphite morphology (Fig. 9).

Fig. 10 shows the deconvoluted high resolution C 1s spectrum of Fe–K/γ-Al_2O_3 catalysts after 300 h of reaction. The XPS spectrum can be deconvoluted into four components, at 283.6, 284.4, 285.1 and 285.9 eV respectively [18,19]. The main peak at 285.9 eV was attributed to the graphite. The peaks at 284.4 and 285.1 were attributed to carbonyl group and deposited hydrocarbons. Fig. 11 shows that the deposited coke showed several absorption bands in the range between 1000 and 4000 cm^{-1}. The band at 3436 cm^{-1} with very strong intensity was assigned to the OH group. The strong bands at 2925 and 2852 cm^{-1} were denoted to symmetric and asymmetric vibration of –CH_2 and –CH groups connected with aromatic carbons. The three bands, in the range between 1750 and 1500 cm^{-1}, were characteristic of the vibration absorption of C=C bonds in aromatic rings. The CH– wagging and twisting modes of

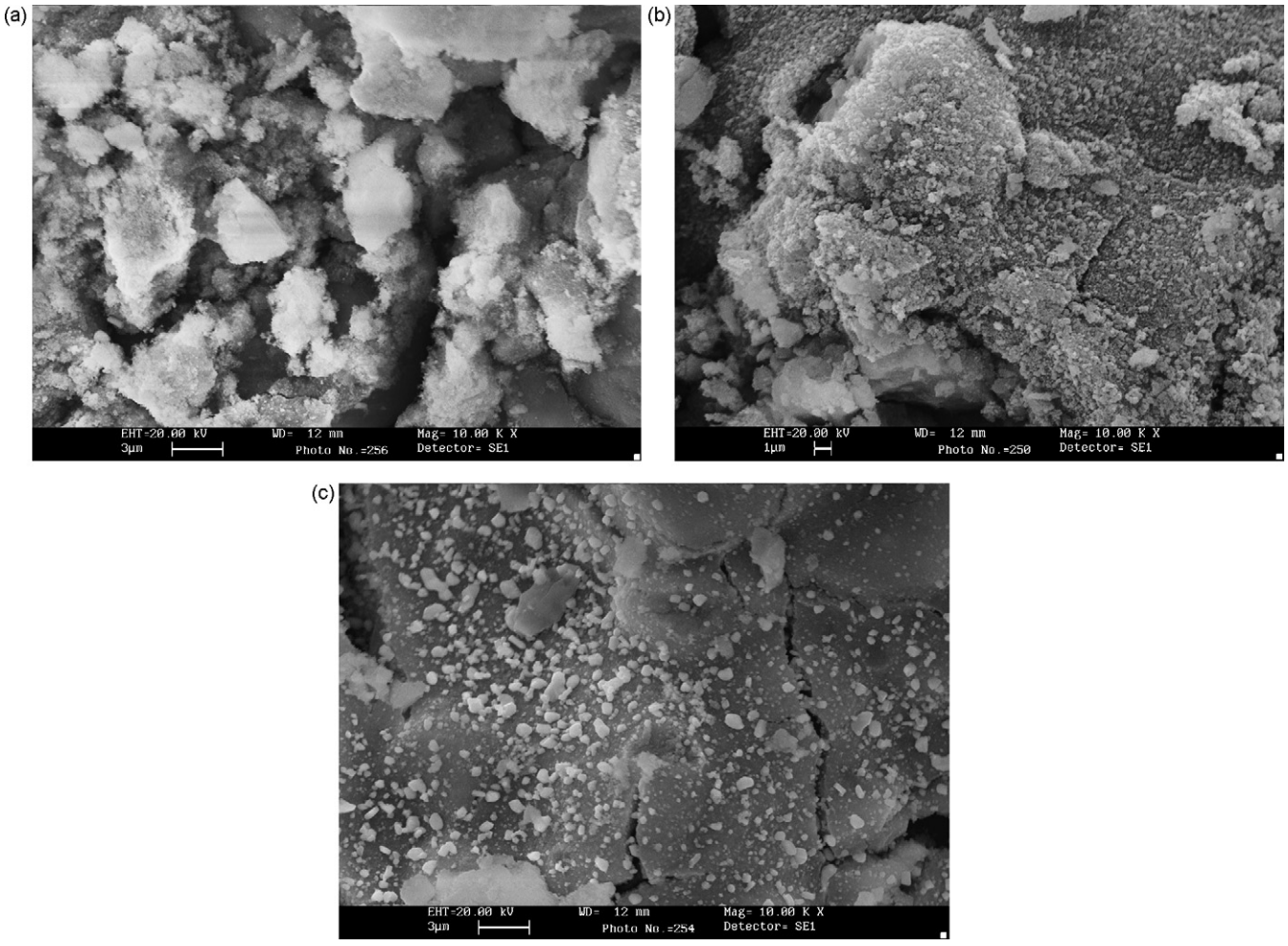

Fig. 9. SEM image of the Fe–K/γ-Al_2O_3 catalysts after CO_2 hydrogenation reaction. (a) 100 h, (b) 300 h, and (c) 500 h.

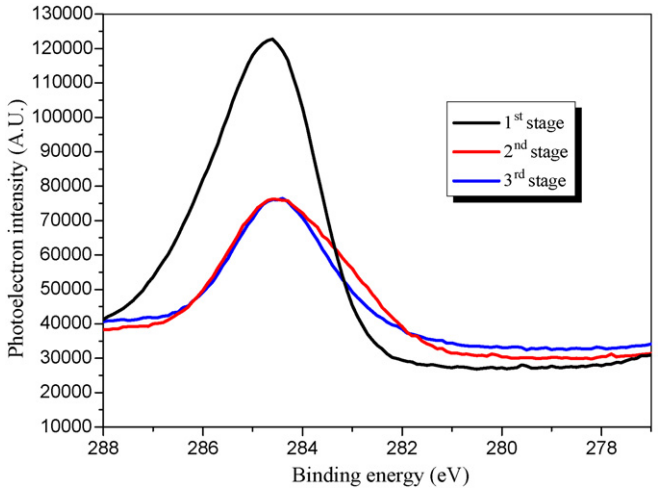

Fig. 10. Carbon 1s XPS spectra of the Fe–K/γ-Al_2O_3 with reactor position.

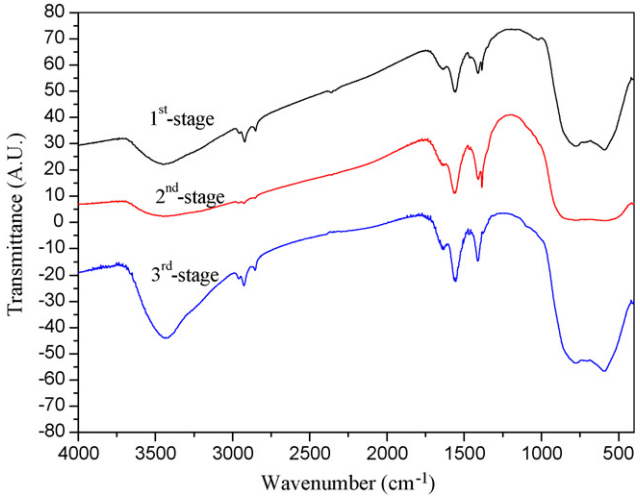

Fig. 11. FT-IR spectra of the Fe–K/γ-Al_2O_3 catalysts after CO_2 hydrogenation reaction for 300 h.

polycyclic aromatics were clearly shown by the bands at 1461, 1374 and 1270 cm^{-1} [16,20]. These results confirmed the presence of both aromatic rings and alkyl groups in the coke sample.

The composition of reactant differed depending on the stage of the catalyst bed. This indicated that coke formation on the catalysts in the 2nd- and 3rd-stage s was related to the different compositions of reactants and products. Compared to the composition in the 1st-stage catalyst bed, the composition in the 2nd- and 3rd-stage catalyst beds had more products and less unconverted reactants. There were also many intermediates in contact with the catalyst in the latter stage catalyst beds. In particularly, the olefins, which were produced in the 1st-stage bed, may easily haven been adsorbed on acidic sites and thus the olefins served as major precursors to coke.

4. Conclusion

The deactivation behavior of Fe–K/γ-Al_2O_3 catalyst was investigated. According to the reaction position and reaction time, the deactivation pathway was different. In the case of phase transformation, the carboneous group was formed by reaction with CO_2, and the carboneous group was transformed to adsorbed CH_2 during CO_2 hydrogenation. Adsorbed CH_2 was converted to χ-carbide over long periods of CO_2 hydrogenation, and finally the χ-carbide was transformed to the stable carbide, which was the deactivated species in CO_2 hydrogenation. The main deactivation reason was the phase transformation at the top of the reactor. Conversely, the main factor at the bottom of the reactor was the deposited coke generated by secondary reactions. Compared to the composition in the 1st-stage catalyst bed, the composition in the 2nd- and 3rd-stage catalyst beds had more products and less unconverted reactants. In particularly, the olefins, which were produced in 1st-stage bed, may easily have been adsorbed on acidic sites and thus the olefins served as major precursors to coke.

References

[1] M.E. Dry, Appl. Catal. A 189 (1999) 185.
[2] G.P. van der Laan, A.A.C.M. Beenackers, Catal. Rev.: Sci. Eng. 41 (1999) 255.
[3] R.A. Dictor, A.T. Bell, J. Catal. 97 (1986) 121.
[4] J.W. Niemantsverdriet, A.M. van der Kraan, W.L. Van Dijk, H.S. Van der Baan, J. Phys. Chem. 84 (1980) 3363.
[5] J.A. Amelse, J.B. Butt, L.H. Schwartz, J. Phys. Chem. 82 (1978) 558.
[6] M.D. Shroff, D.S. Kalakkad, K.E. Coulter, S.D. Kohler, M.S. Harrington, N.B. Jackson, A.G. Sault, A.K. Datye, J. Catal. 156 (1995) 185.
[7] H.B. Zhang, G.L. Schrader, J. Catal. 95 (1985) 325.
[8] J. Hwang, K. Jun, K. Lee, Appl. Catal. A 208 (2001) 217.
[9] D.B. Bukur, X. Lang, J.A. Rossin, W.H. Zimmerman, M.P. Rosynek, E.B. Yeh, C. Li, Ind. Eng. Chem. Res. 28 (1989) 1130.
[10] S.A. Eliason, C.H. Bartholomew, Appl. Catal. A 186 (1999) 229.
[11] M. Pijolat, V. Perrichon, P. Bussiere, J. Catal. 107 (1987) 82.
[12] B.S. Liu, L.T. Au, Appl. Catal. A 244 (2003) 181.
[13] H. Ando, Q. Xu, M. Fujiwara, Y. Matsumura, M. Tanaka, Y. Souma, Catal. Today 45 (1998) 229.
[14] S.K. Sahoo, P.V.C. Rao, D. Rajeshwer, K.R. Krishnamurthy, I.D. Singh, Appl. Catal. A 244 (2003) 311.
[15] J. Li, X. Zhan, Y. Zhang, G. Jacobs, T. Das, B.H. Davis, Appl. Catal. A 228 (2002) 203.
[16] C.L. Li, O. Novaro, X. Bokhimi, E. Muñoz, J.L. Boldú, J.A. Wang, T. López, R. Gómez, N. Batina, Catal. Lett. 65 (2000) 209.
[17] J. Zhang, A. Schneider, G. Inden, Corros. Sci. 45 (2003) 281.
[18] Z. Zhang, X.E. Verykios, S.M. MacDonald, S. Affrossman, J. Phys. Chem. 100 (1996) 744.
[19] R. Rajagopalan, J.O. Iroh, Appl. Surf. Sci. 218 (2003) 58.
[20] E. Guglielminotti, J. Phys. Chem. 98 (1994) 9033.